

Comparing the accuracy of full-arch implant impressions using the conventional technique and digital scans with and without prefabricated landmarks in the mandible: An *in vitro* study

Yifang Ke¹, Yaopeng Zhang¹, Yong Wang, Hu Chen^{*}, Yuchun Sun^{*}

Center of Digital Dentistry, Peking University School and Hospital of Stomatology & National Engineering Research Center of Oral Biomaterials and Digital Medical Devices & National Center of Stomatology & National Clinical Research Center for Oral Diseases & Beijing Key Laboratory of Digital Stomatology & Research Center of Engineering and Technology for Digital Dentistry Ministry of Health, Beijing, China

ARTICLE INFO

Keywords:

Accuracy
Conventional implant impression
Digital scans
Full-arch implant impression
Prefabricated landmarks

ABSTRACT

Objectives: This study evaluated the accuracy of digital implant impressions with or without prefabricated landmarks compared with the conventional method in the edentulous mandible.

Methods: An edentulous mandibular stone cast with implant abutment analogs and scan bodies in FDI #46, #43, #33, and #36 served as the master model. The scans captured with intraoral scanners (IOS) were divided into four groups: IOS-NT (no landmarks + Trios 4 scanner), IOS-NA (no landmarks + Aoralscan 3 scanner), IOS-YT (landmarks + Trios 4 scanner), and IOS-YA (landmarks + Aoralscan 3 scanner) (n=10). Landmarks were attached to the scan bodies with resin to improve scanning fluency. Conventional open-trayed technique (CNV) was performed with the 3D-printed splinting frameworks (n=10). The master model and conventional castings were scanned using a laboratory scanner, and the former served as the reference model. Overall distance and angle deviations between scan bodies were measured to determine trueness and precision. The ANOVA or Kruskal–Wallis test compared CNV group to scans without landmarks, while a generalized linear model analyzed scan groups with and without landmarks.

Results: Compared to the CNV group, the IOS-NA and IOS-NT groups showed higher overall distance trueness (p=0.009), and precision (distance, p<0.001 and angular, p<0.001). With landmarks, the IOS-YA group had higher overall trueness (distance, p<0.001 and angular, p<0.001) than the IOS-NA group, and the IOS-YT group has higher distance trueness (p=0.041) than the IOS-NT group. Moreover, the precision in distance and angle was significantly improved for IOS-YA and IOS-YT groups, compared with the IOS-NA (p<0.001) and IOS-NT (p<0.001) groups separately.

Conclusions: Digital scans were more accurate than conventional splinting open-trayed impressions. Prefabricated landmarks significantly improved the accuracy of full-arch implant digital scans, regardless of the scanner used.

Clinical significance: Prefabricated landmarks can enhance the accuracy of intraoral scanners for full-arch implant rehabilitation, improving scanning efficiency and clinical outcomes.

1. Introduction

Implant-supported complete dental prostheses are indispensable and reliable options for edentulous jaws [1]. Taking impressions is the first step in the production process of implant-supported prostheses. Inaccurate impressions result in a misfit between the prosthesis and implant abutment, which may lead to mechanical and biological complications that affect the long-term of the implants [2,3]. Thus, accurate

impressions are critical to prostheses that are supported by multiple implants.

Conventional open-trayed impression of multiple implants is one of the most widely used strategies. During this procedure, the impression copings are splinted to prevent them from rotation movements. Therefore, this method is recommended over the non-splinting technique [4, 5]. However, this workflow is complex, inefficient, and requires substantial clinical experience. It is recommended for experienced dentists

^{*} Corresponding authors.

E-mail addresses: ccen@bjmu.edu.cn (H. Chen), kqsy@bjmu.edu.cn (Y. Sun).

¹ These authors contributed equally to this work.

only, as inexperienced dentists have been found to have a significantly higher rate of unsuccessful results when using the splinting technique [6]. Moreover, during the conventional workflow, several factors may affect the accuracy of the implant impressions, such as patients' pharyngeal reflex and the potential deformation of the impression materials.

As computer-aided design/computer-aided manufacturing (CAD/CAM) and digital technologies have flourished, the intraoral scanner (IOS) has become increasingly popular for acquiring implant positions. IOSs are comfortable, efficient, and practical for clinical use. However, IOSs cannot replace all standard practices. Regarding implant-supported fixed dental prostheses, intraoral scanners can be used in single- and three-unit implant scanning [7,8]. In 2020, Revell et al. recommended certain scanners, such as Primescan, for complete-arch implant impressions based on the low deviation values at the implant platform level [9]. However, the accuracy of older models of intraoral scanners is not reliable for scanning edentulous spaces with long inter-implant distances or fully edentulous jaws [7,10–12], especially for inexperienced operators [9,13].

Previous studies have placed auxiliary devices in the edentulous area or custom-designed scan bodies with an extensional structure to obtain reliable digital full-arch implant impressions [14–17]. These platforms usually require custom-made scan bodies or a second scan to obtain mucosal information. In this study, newly designed prefabricated landmarks were produced. The lack of geometric variation can be overcome by adding landmarks with letter patterns between the scan bodies, providing a solution for the digital implant impression of edentulous jaws. As the prefabricated landmarks do not block the mucosa, only one scan is required. This study aimed to evaluate the accuracy of digital implant impressions in edentulous jaws with or without prefabricated landmarks compared to conventional impressions. Null hypothesis 1: There would be no significant difference in the accuracy between digital impressions with or without prefabricated landmarks tested in two intraoral scanners. Null hypothesis 2: There would be no significant difference in the accuracy between digital impressions without landmarks and conventional impressions.

2. Materials and methods

Ethics approval was not required for this *in vitro* study.

2.1. Reference data

An edentulous mandibular stone cast with a gingival replica was used as the master model. Four implant abutment analogs (Abutment Replica Multi-unit RP system, Nobel, Zurich, Switzerland) were implanted in the right first molar (FDI #46), right canine (FDI #43), left canine (FDI #33), and left first molar (FDI #36) positions numbered

1–4. Four scan bodies (NB MU-R Scan body, Segma, Beijing, China) were then mounted and tightened to 15 Ncm to the implant abutment analogs using a torque wrench (Fig. 1a).

The mandibular stone cast model without landmarks was scanned using a laboratory scanner with a precision of 2.9 μm and trueness of 12.8 μm (T710, Medit, Seoul, Korea) (Table 1) as the reference model [18]. Datasets from the scans were exported to the Standard Tessellation Language (STL) file format.

2.2. Design and fabrication of prefabricated landmarks

The edentulous mandibular stone cast with prefabricated landmarks was shown in Fig. 1b. The landmark was composed of three components: a collar, a long plate, and a connecting cylinder with a 45–60° angle to the horizontal plane that linked the collar and the long plate (as seen in Fig. 2a). The long plate was in the shape of a cuboid and had various protruding letter patterns, which enhanced the curvature change. The collar was used to connect to the scan body (as shown in Fig. 2a and b). The design of these landmarks was created using 3D mechanical design software (Solidworks 2020, Dassault Systemes, Paris, France) (Fig. 2a). The prototypes were then produced using a 3D printing machine (AccuFab-L4D, Shining 3D, Hangzhou, China) with opaque UV-sensitive resin (DM11, Shining 3D, Hangzhou, China) (as shown in Fig. 2b). The post-processing steps included removing the support, washing, and UV light curing according to the guideline of the manufacturer. Before use, these landmarks could be adjusted using the handpieces to match the inter-implant distance.

2.3. Intraoral scanning procedures

Two intraoral scanners were used for the IOS group specimens: Trios 4 (Trios 4, 3Shape A/S, Copenhagen, Denmark) and Aoralscan 3 (Aoralscan 3, Shining 3D, Hangzhou, China). The hardware and software versions of the scanners are listed in Table 1. Four subgroups were created based on whether landmarks were to be added as well as the type of intraoral scanner. The resultant subgroups were IOS-NT (no landmarks + Trios 4 scanner), IOS-NA (no landmarks + Aoralscan 3 scanner), IOS-YT (landmarks + Trios 4 scanner), and IOS-YA (landmarks + Aoralscan 3 scanner). The workflow used in this study is shown in Fig. 3. For the IOS-NT and IOS-NA groups, the reference stone model

Table 1

The hardware and software versions of scanners used.

Scanner	Manufacturer	Software version
Medit T710	Medit	2.5.6.193
Trios 4	3Shape A/S	1.7.27.6
Aoralscan 3	Shining 3D	V1.0.0.3030

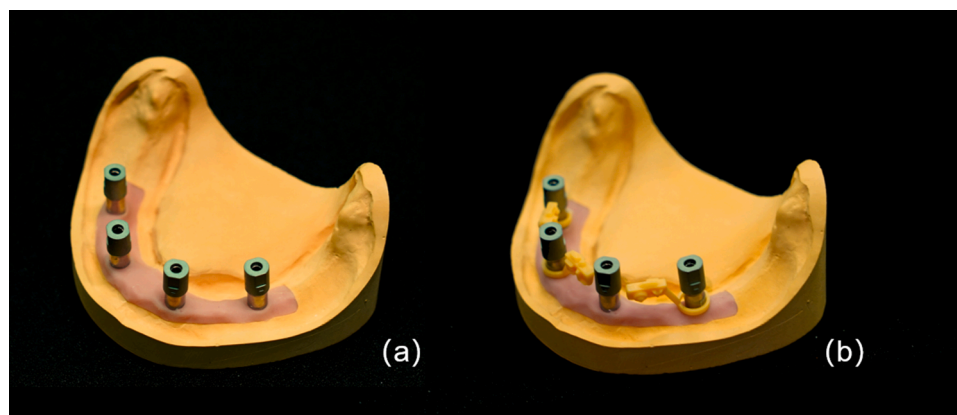


Fig. 1. (a) The reference mandibular typodont; (b) The reference mandibular typodont with prefabricated landmarks.

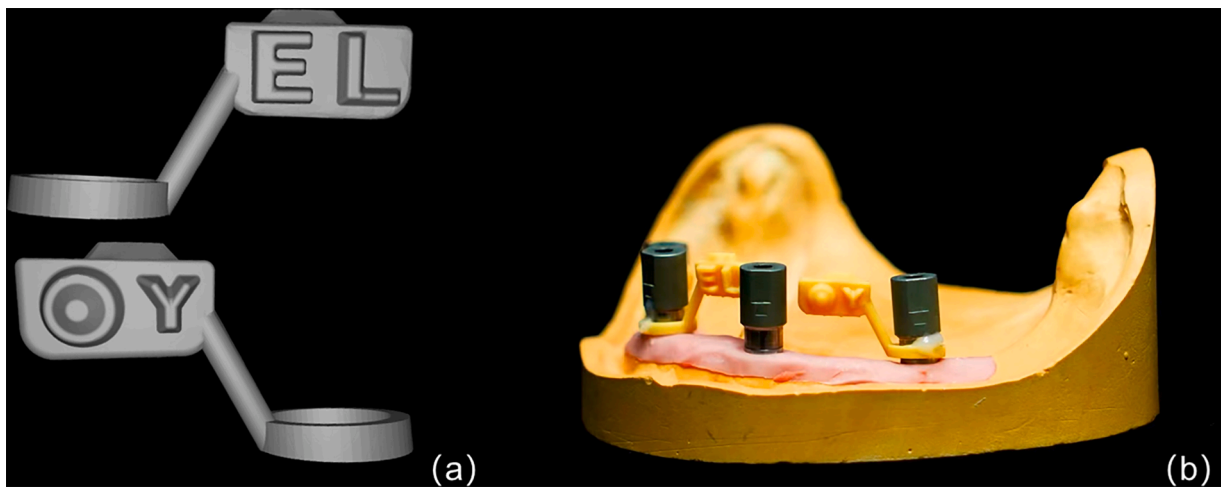


Fig. 2. The prefabricated landmarks. (a) The CAD model of landmarks; (b) Landmarks were attached to scan bodies using resin.

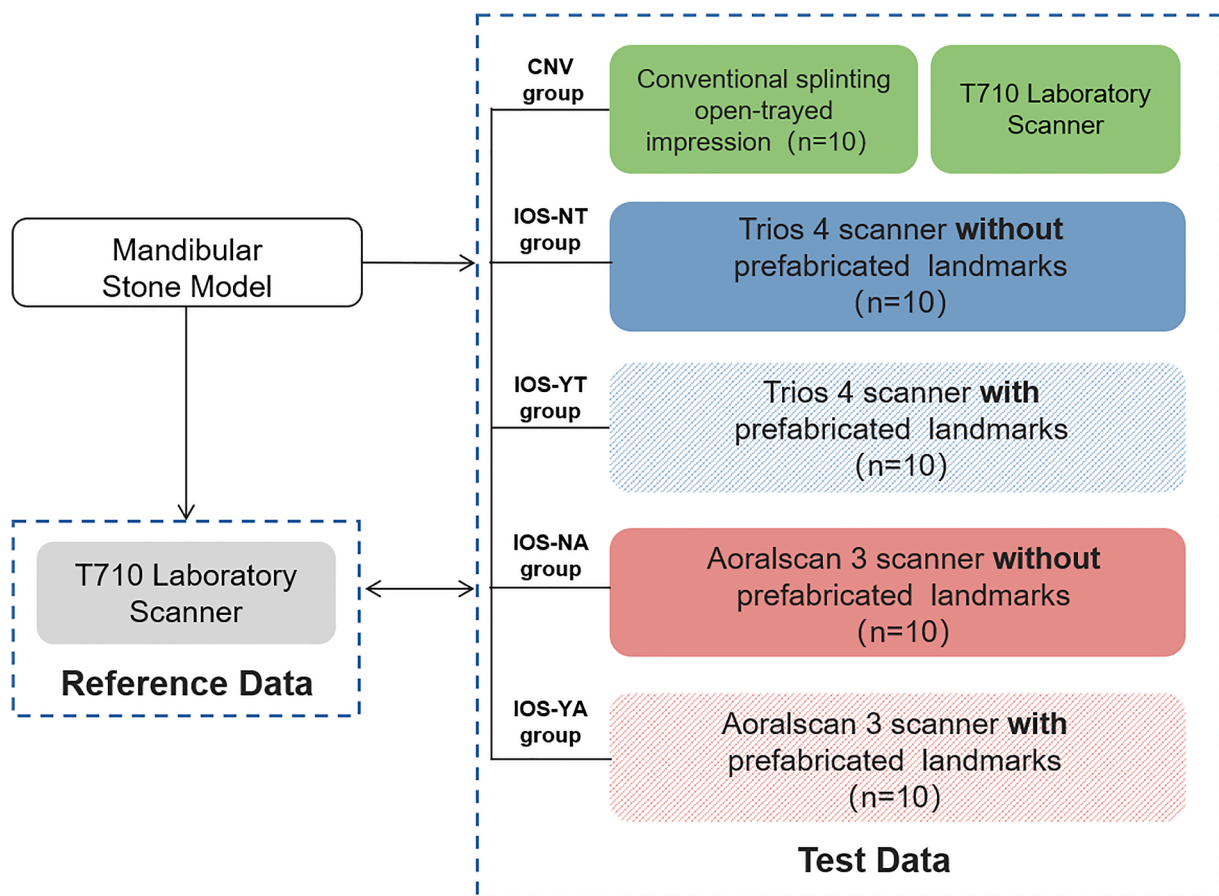


Fig. 3. Workflow of the study.

was scanned 10 times using the Trios 4 and Aoralscan 3 scanners, resulting in 20 STL files. Subsequently, the collars were placed on the bottom of the scan bodies and the long plates were free to be rotated around the scan body at any angle. After rotating the long plate to the edentulous area between the scan bodies, the collars were attached to the scan body with resin (TempoCemNE, DMG, Hamburg, Germany). The scan bodies were not removed during the whole process. The same scanning procedure was repeated for the IOS-YT and IOS-YA, and 20 STL files were produced. All scans were performed by an intraoral scanner operator with more than one and a half years of experience. To ensure

consistency and accuracy, the humidity and temperature conditions were kept the same for all scanning procedures. Before beginning the scans, both the laboratory and intraoral scanners were calibrated according to the manufacturer's guidelines. During calibration, the tip was gently slid off from the intraoral scanner, the calibrator was connected to the front of the scanner, and the calibration process was completed using the supplied software. The scanning procedure always started at the left first molar and ended at the right first molar, with the scanning path following specific order: occlusion, buccal, and lingual. All steps were performed by the manufacturer's recommendations to ensure the

highest quality results.

2.4. Conventional procedures

For CNV group specimens, a splinting open-trayed implant impression technique was used as the control group. Based on the location of the implant abutment analogs, the splinting framework (collars and bars) and custom-made impression trays were designed. This process was completed using Solidworks software (Solidworks 2020, Dassault Systemes, Paris, France). Once the design was finalized, the splinting frameworks and impression trays were fabricated using a 3D printing machine (AccuFab-L4D, Shining 3D, Hangzhou, China) in opaque UV-sensitive resin material (DM11, Shining 3D, Hangzhou, China) (Fig. 4a–c). Four impression copings (Impression Coping Open-tray Multi-unit RP System, Nobel, Zurich, Switzerland) were positioned and tightened onto implant abutment analogs of mandibular typodont using a torque wrench, with a force of 15 Ncm. The splinting framework was then connected to the copings with resin (TempoCemNE, DMG, Hamburg, Germany) (Fig. 4d). Light-body polyvinyl siloxane impression materials (Type 3 Light Body, HUGE, Shanghai, China) were applied under the resin stent and around the gingival aspects of the impression copings. Then, an open-tray filled with heavy-body impression material (Type 0 Heavy Body, HUGE, Shanghai, China) was inserted so that the long screws were extruded. After polymerization for four minutes, the impression was removed from the model, and another four analogs were engaged in impression copings using long screws. Subsequently, the impression was cast using a dental stone (Type IV Die-Stone, Heraeus, Hanau, Germany) to create a definitive conventional stone cast (Fig. 4e). This procedure was repeated ten times. Stone casts were stored for a week before scanning. Subsequently, the stone casts were fitted with the same scan bodies, scanned using a laboratory scanner (T710, Medit, Seoul, Korea), and exported as STL files.

2.5. Measurements

For accuracy assessment, the scan files were imported into a 3D metrology software (Geomagic Control X 2018, 3D Systems, Rock Hill, USA). Each boundary of the scanned model was automatically segmented using software according to the curvature change (setting the curvature sensitivity to 65). The four scan bodies were selected as the registration area, each test model was aligned to the reference model using the best-fit algorithm.

Subsequently, the software automatically detected the geometry of the scan bodies and created cylinders and their central axes, as well as planes to represent the upper surface of each scan body (Fig. 5a). The central point of the scan body was determined by the intersection of a cylinder axis and a plane. As a result, central points and axes were established for all four scan bodies (Fig. 5a). Angle measurements were done between the central axis of cylinders 1–2, 1–3, and 1–4 (Fig. 5b), and the distance measurements were done between the central point of cylinders 1–2, 1–3, and 1–4 (Fig. 5c). This accuracy methodology had been widely used in the previous study [11,16,19,20].

According to ISO 5725, accuracy consists of “trueness” and “precision” (ISO-Norm 5725–1:1994 “Accuracy (trueness and precision) of measurement methods and results—Part 1: General principles and definitions”). Trueness referred to the absolute value of the distance and angle deviations between the reference model and scanned model, $n=10 \times 5$ (groups)=50. Precision referred to the absolute deviation in the test data between pairs in each group, $n=C_{10}^2 \times 5$ (groups)=225. The deviation (Δd) of every span was considered as Δd_{12} , Δd_{13} , and Δd_{14} , and the overall deviation was considered as follows:

$$\Delta d_{\text{overall}} = \Delta d_{12} + \Delta d_{13} + \Delta d_{14}$$

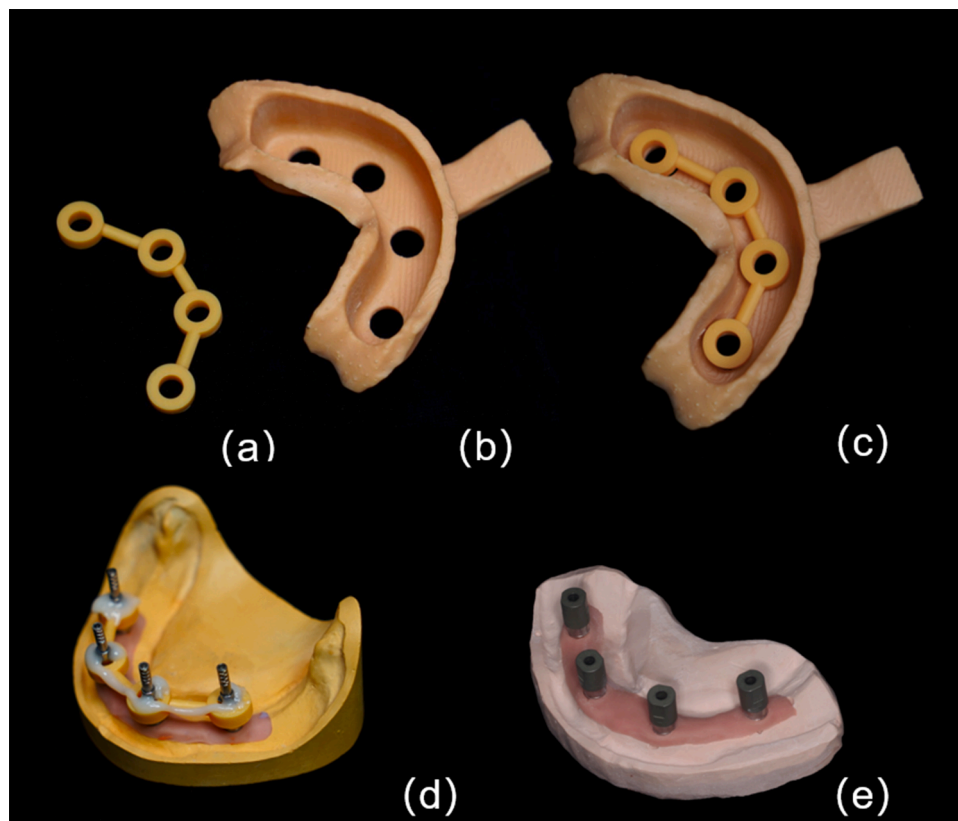


Fig. 4. Conventional splinting open-trayed technique. (a) 3D-printed splinting framework; (b) 3D-printed custom open-tray; (c) 3D-printed splinting framework inside custom open-tray; (d) Splinting framework and copings were connected with resin; (e) The conventional stone casting with the same scan bodies.

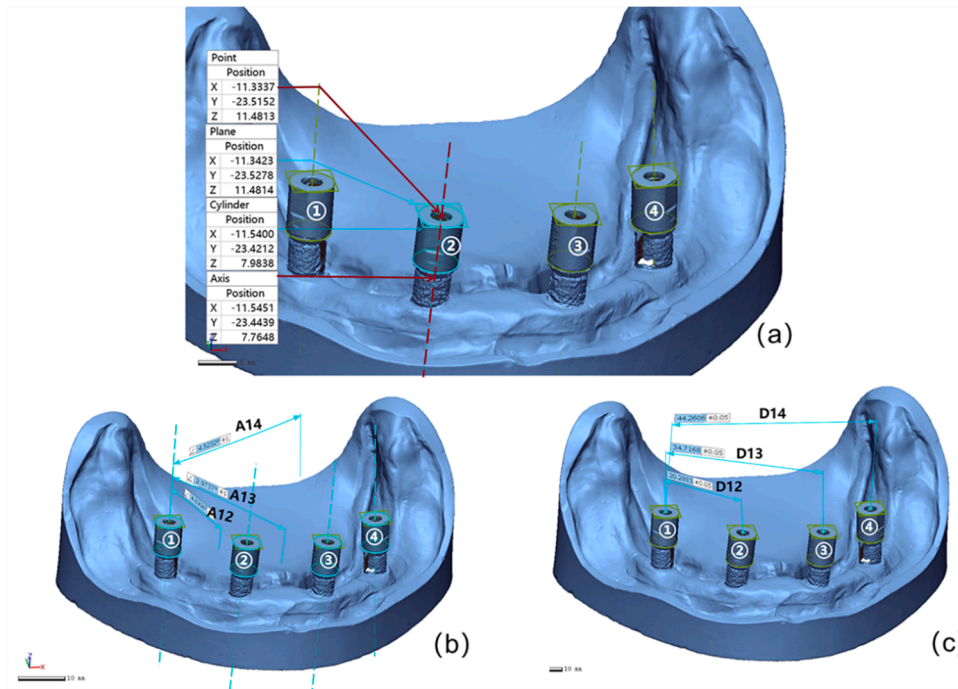


Fig. 5. Calculation method of distances and angles. (a) Scan bodies in the STL data set transferred to standard cylinder geometries, planes, and create central axes and points; (b) angles were defined by intersecting the central axis of cylinders 1-2, 1-3, 1-4; (c) distances were defined by linking points 1-2, 1-3, 1-4.

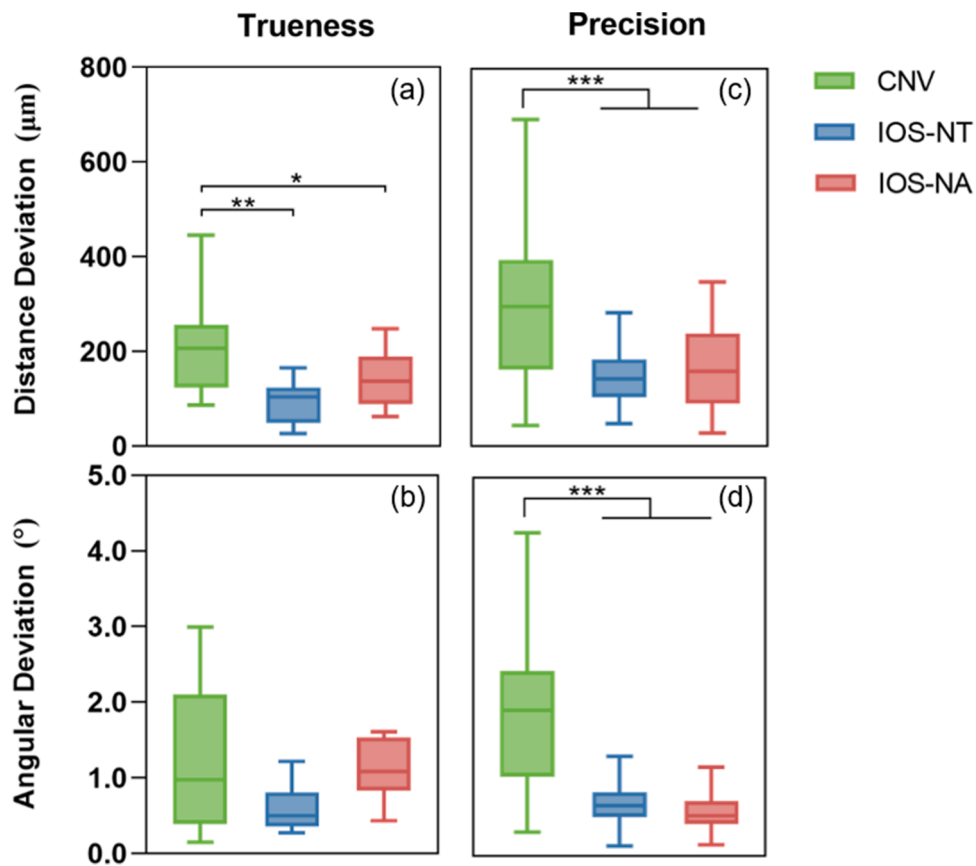


Fig. 6. Median, interquartile range, and range of the accuracy in angle and distance of CNV and IOS groups without landmarks. (a) Distance trueness; (b) Angular trueness; (c) Distance precision; (d) Angular precision. CNV, conventional group; IOS-NT, Trios 4 scanner without landmarks; IOS-NA, Aoralscan 3 scanner without landmarks. * indicates Bonferroni adjusted significance (* $p < 0.05$, ** $p < 0.01$, *** $p < 0.001$).

2.6. Statistical analysis

Statistical calculations were performed using SPSS software (SPSS Statistics 24, IBM, Armonk, USA). Four measurement results were run separately: overall trueness of distance and angle, and overall precision of distance and angle. The Shapiro–Wilk and Levene tests were used to detect data normality and variance homogeneity, respectively. The statistical analysis was divided into two parts. First, the CNV group was compared with the two digital impressions without landmark groups to assess the accuracy of different implant impression technologies. The one-way ANOVA or Kruskal–Wallis test was used, depending on the normality and homogeneity of the data. The Shapiro–Wilk test revealed that the data were normally distributed. According to the Levene test, only the groups in distance trueness showed homogeneity of variances, whereas the other groups showed heterogeneous variances. Thus, the one-way ANOVA test was used in the distance trueness evaluation, and the Kruskal–Wallis test was used by the other groups. Secondly, to compare the influence of the prefabricated landmarks on the accuracy, data from the IOS-NT, IOS-YT, IOS-NA, and IOS-YA groups were analyzed using a generalized linear model. Landmarks and scanners were the main comparative factors, and their interactions were integrated into the model. P values were adjusted using the Bonferroni method for pairwise comparisons. The inspection level was two-sided ($\alpha=0.05$).

3. Results

3.1. Comparison of conventional technique and digital scans without landmarks

The results of the overall distance and angular deviations for the conventional technique and digital scans without landmarks (IOS-NT and IOS-NA groups) were shown in Fig. 6, Tables 2 and 3. As for trueness, the one-way ANOVA showed that a significant difference was found in distance trueness ($p=0.009$). The conventional group showed the highest overall distance deviation, compared with the IOS-NA ($p=0.048$) and IOS-NT ($p=0.002$) groups, however, no significant difference was found among these three groups in angular trueness ($p=0.051$). Both the precision of angle and distance from the IOS-NT ($p<0.001$) and IOS-NA ($p<0.001$) groups were significantly better than those from the CNV group.

3.2. Comparison of digital scans with or without landmark

The results of the overall distance and angular deviations from the digital scans with or without landmark groups were shown in Fig. 7, Tables 2 and 3. Results of the normality and homogeneity of variance tests varied from one case to another, as detected by the Shapiro–Wilk test and the Levene test, respectively. From the generalized linear model, the use of landmarks demonstrated statistical significance ($p<0.001$) in all the trueness and precision results (Tables 4 and 5).

Considering the effect of landmark placement in the model, as for trueness, the pairwise comparison revealed that statistically significant differences were found between the IOS-NA and IOS-YA groups in both

the overall trueness (distance, $p<0.001$ and angular, $p<0.001$), and the IOS-YT group presented significantly higher trueness than the IOS-NT group in distance deviations ($p=0.041$) (Fig. 7). As for the precision of distance and angular, the IOS-YA and IOS-YT groups were more precise than the IOS-NA ($p<0.001$) and IOS-NT ($p<0.001$) groups separately (Fig. 7).

Considering the effect of intraoral scanners used in the study, the IOS-NT group showed higher trueness (distance, $p=0.019$ and angular, $p<0.001$) and distance precision ($p=0.040$) than the IOS-NA group (Fig. 7). With the landmarks in place, however, the IOS-YA group revealed significantly higher overall angular trueness ($p=0.023$), and precision (distance, $p=.004$ and angular, $p<0.001$) than the IOS-YT group (Fig. 7).

4. Discussion

The results indicated that the first and second null hypotheses were rejected because digital scans, even without prefabricated landmarks, exhibited better accuracy than the conventional method. Significant differences were detected between the IOS-NT and IOS-YT groups, as well as between the IOS-NA and IOS-YA groups, for both trueness and precision.

The accuracy of the digital impressions is greatly influenced by the inter-implant distance and scan range [12]. Previous studies showed that the accuracy of digital scans in all-on-6 was significantly lower than that of all-on-8, which was primarily related to the short inter-implant distance in all-on-8 [10]. Another study found that when the scanning range was across the entire dental arch in the all-on-8 model, the scanning accuracy was greatly reduced [11]. Miyoshi et al. suggested that intraoral scanners can be used in a 3-unit superstructure supported by two implants [7]. This can be explained by the largest cumulative errors at the largest distance, as well as the errors caused by the lack of noticeable changes in the mucosal curvature during the image-stitching process [21]. In this study, landmark-assisted intraoral scanning ameliorated this situation.

Several studies have been conducted to enhance the accuracy of intraoral scanners in edentulous areas. Mizumoto et al. evaluated the accuracy of four scanning techniques on the all-on-4 model: no modification, the use of glass fiducial markers, brushing pressure-indicating paste, and floss tied between the scan bodies [17]. Compared to the no-modification method, the scanning techniques assisted by various surface treatments revealed similar distance deviations. However, Kim et al. placed a 4 × 3 mm alumina landmark on an edentulous area that spans 26 mm. The accuracy of digital scans was improved significantly, considering that the mean precision was 9.2 to 12.4 μm [22]. This highlights the importance of incorporating three-dimensional structures in the edentulous area for improved accuracy of digital impressions. Huang et al. also explored the use of newly designed scan bodies with extensional structures [14]. Iturrate et al. designed an auxiliary geometry that mimicked a non-edentulous jaw, which provided more accurate results [16]. However, this method required two scans. This study offers a more convenient solution with the use of prefabricated landmarks. These landmarks do not obstruct the mucous membrane, allowing for highly accurate digital impressions of multi-implant

Table 2

Median, interquartile range (IQR), mean, standard deviation (SD) of trueness in distance and angle of CNV, IOS-NT, IOS-YT, IOS-NA, and IOS-YA groups.

	Distance (μm)				Angle (°)			
	Median	IQR	Mean	SD	Median	IQR	Mean	SD
CNV	206.1	131.5	207.4	103.8	1.0	1.7	1.2	1.0
IOS-NT	103.4	74.8	96.7	43.8	0.5	0.5	0.6	0.3
IOS-YT	54.5	48.1	59.9	27.6	0.4	0.2	0.4	0.2
IOS-NA	136.8	100.9	139.0	60.9	1.1	0.7	1.1	0.4
IOS-YA	76.6	44.8	74.5	28.8	0.1	0.2	0.2	0.1

CNV, conventional group; IOS-NT, Trios 4 scanner without landmarks; IOS-YT, Trios 4 scanner with landmarks; IOS-NA, Aoralscan 3 scanner without landmarks; IOS-YA, Aoralscan 3 scanner with landmarks.

Table 3

Median, interquartile range (IQR), mean, standard deviation (SD) of precision in distance and angle of CNV, IOS-NT, IOS-YT, IOS-NA, and IOS-YA groups.

	Distance (µm)				Angle (°)			
	Median	IQR	Mean	SD	Median	IQR	Mean	SD
CNV	295.5	231.6	280.2	141.8	1.9	1.4	1.9	1.0
IOS-NT	143.2	79.6	142.8	57.8	0.7	0.3	0.7	0.3
IOS-YT	75.2	50.9	81.5	43.0	0.4	0.3	0.4	0.2
IOS-NA	158.5	148.5	168.5	91.1	0.5	0.3	0.6	0.2
IOS-YA	46.8	43.7	45.5	28.0	0.2	0.2	0.2	0.1

CNV, conventional group; IOS-NT, Trios 4 scanner without landmarks; IOS-YT, Trios 4 scanner with landmarks; IOS-NA, Aoralscan 3 scanner without landmarks; IOS-YA, Aoralscan 3 scanner with landmarks.

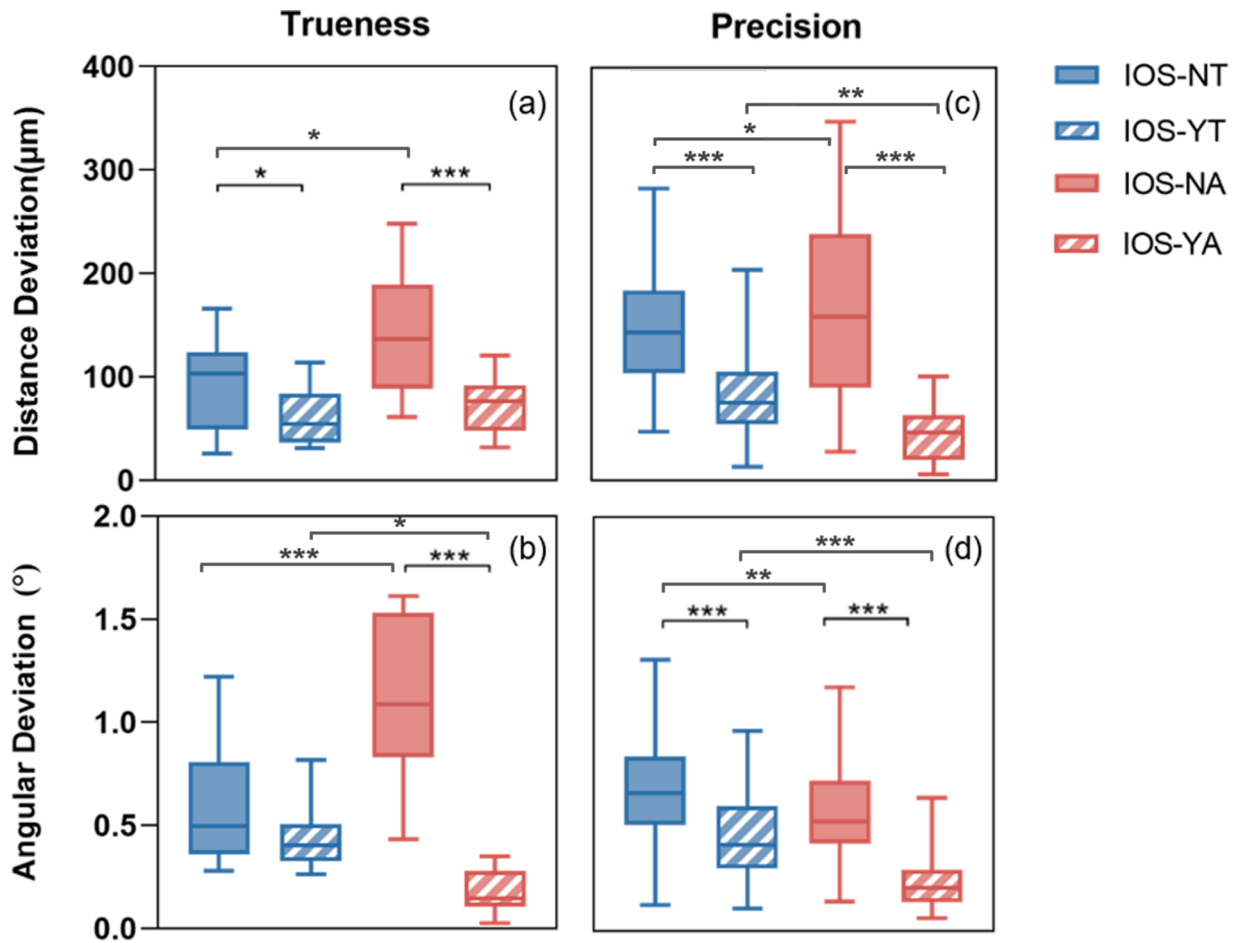


Fig. 7. Median, interquartile range, and range of the accuracy in angle and distance of IOS groups with or without landmarks. (a) Distance trueness; (b) Angular trueness; (c) Distance precision; (d) Angular precision. IOS-NT, Trios 4 scanner without landmarks; IOS-YT, Trios 4 scanner with landmarks; IOS-NA, Aoralscan 3 scanner without landmarks; IOS-YA, Aoralscan 3 scanner with landmarks. * indicates Bonferroni adjusted significance (* $p < 0.05$, ** $p < 0.01$, *** $p < 0.001$).

Table 4

Generalized linear model results for trueness analysis of digital impressions.

Dependent variable: overall deviation Source	Distance		Angle	
	χ^2	p	χ^2	p
Landmark	15.832	< 0.001	46.781	< 0.001
Scanner	4.992	.025	2.311	.129
Landmark*Scanner	1.183	.277	22.366	< 0.001

Significance at $p < 0.05$.

edentulous jaws with just one scan. Unlike commercial devices, such as the Nexus iOS system by Osteon, or custom-made scan bodies, the pre-fabricated landmarks do not alter the structure of the scan bodies, eliminating the need to build a digital library in CAD software. Additionally, the landmarks can be adjusted by the handpiece to adapt to any

Table 5

Generalized linear model results for precision analysis of digital impressions.

Dependent variable: overall deviation Source	Distance		Angle	
	χ^2	p	χ^2	p
Landmark	109.415	< 0.001	74.650	< 0.001
Scanner	.346	.556	24.614	< 0.001
Landmark*Scanner	12.239	< 0.001	1.703	.192

Significance at $p < 0.05$.

implant location.

Based on the principle of intraoral scanners, a single 3D image is created by stitching multiple 2D images [23,24]. Through similarity calculations, the software determines where there are co-occurring points of interest (POI) in two images [25]. These POIs can be

detected by transition zones such as physical limitations, strong curvatures, or differences in gray intensities [26]. Without prefabricated landmarks, the flat and uniform edentulous area confused the detection of POIs. Therefore, the registration of the overlapping regions was prone to error. In contrast, the prefabricated landmarks enriched the curvature variations of the edentulous spaces, allowing intraoral scanners to obtain more reliable POIs to distinguish between the mucosa images with similar shapes.

For accuracy studies, reference data are obtained using coordinate measuring machines (CMM) or laboratory scanners. The CMM measures the coordinates of the spatial points on the surfaces of the model with submicrometre accuracy. However, it cannot obtain full-surface 3D point clouds of the model [27]. Laboratory scanners provide complete surface morphology that has been widely used in previous studies [7,11,14,15,22,28,29]. Besides, Borbola et al. suggested that some novel laboratory scanners, such as Medit T710 (with a precision of 2.9 μm and trueness of 12.8 μm), were suitable for accuracy studies due to their comparable precision to an industrial scanner [18]. Therefore, Medit T710 was selected as the reference scanner for this study. In addition, the accuracy assessment of the four digital groups and the conventional group was performed using the distance and angular deviations instead of the RMS values. The measurement of the RMS values requires best-fit alignment algorithms that make the test and reference data as close as possible to the corresponding theoretical data. Therefore, distances may be averaged over the entire surface, and the deviation between the images may be underestimated after superimposition [7,30]. When larger and more different data were applied, such as the all-edentulous jaws used in this experiment, the influence of the error was greater [31]. In contrast, the distance and angular deviations calculate the discrepancy of inter-implants between the reference and test data, which has been suggested by several studies [11,16,19,32,33]. The limitation of this measurement is that the height of the scan body may influence the results because prosthesis fit should occur at the platform level [9]. Nevertheless, platform deviations can be calculated using the known height.

Prefabricated plastic or metallic frameworks were suggested to reduce the effects of dimensional changes in implant impression splinting techniques [34–36]. 3D-printed framework was more dimensionally stable and less time-consuming than dental floss [34,36,37], which was selected in the present study. Based on the present research, however, digital scans exhibited higher accuracy relative to the conventional splinting open-trayed impression technique. This might be explained by the fact that the splinting techniques add complexity to the process of making conventional impressions, which was technique-sensitive and required substantial clinical experience from the operator [6]. In addition, the two intraoral scanners employed in this study are of the latest model, featuring hardware and software advancements. They offer reliable accuracy regardless of the operator's level of expertise. Besides, the auxiliary landmarks improved digital scanning fluency, especially in cross-arch and edentulous scanning. Thus, these landmarks may make it easier for the less experienced operators.

This study has some limitations. During scanning, the mandibular stone model was stable and static. During the actual treatment process, the gingival and mucous membranes of edentulous patients are influenced by the activities of the tongue, frenulum, buccal muscles, and other tissues, resulting in residual shadows during scanning. Further, *in vivo* experiments are required to verify this accuracy. In addition, the prefabricated landmarks needed to be attached to the scan bodies, which required a waiting time in the clinic as the resin cured. One approach to reducing the time spent *in vivo* is to bond the landmarks and scan bodies before mounting. Furthermore, better connection methods and designs are necessary.

5. Conclusions

Considering the limitations of this *in vitro* study, the key findings are as follows.

- 1 Digital scans, even without prefabricated landmarks, exhibited better accuracy than the conventional method.
- 2 By using prefabricated landmarks, the accuracy of digital implant impressions in the edentulous mandibular jaw was significantly increased, as observed for both the Aoralscan 3 and Trios 4 scanning systems.

CRedit authorship contribution statement

Yifang Ke: Conceptualization, Methodology, Software, Data curation, Validation, Formal analysis, Investigation, Writing – original draft, Visualization. **Yaopeng Zhang:** Methodology, Software, Validation, Formal analysis, Investigation, Writing – original draft. **Yong Wang:** Writing – review & editing, Supervision. **Hu Chen:** Conceptualization, Methodology, Software, Resources, Writing – review & editing, Supervision, Funding acquisition. **Yuchun Sun:** Conceptualization, Methodology, Software, Resources, Visualization, Project administration, Funding acquisition.

Declaration of Competing Interest

The authors declare that they have no known competing financial interests or personal relationships that could have appeared to influence the work reported in this paper.

Acknowledgments

The research was supported by the National Key R&D Program of China (2019YFB1706900); Beijing Training Project for the Leading Talents in S&T (Z191100006119022); Capital's Funds for Health Improvement and Research (2022-2Z-4106).

References

- [1] P. Papaspyridakos, M. Mokti, C.J. Chen, G.I. Benic, G.O. Gallucci, V. Chronopoulos, Implant and prosthodontic survival rates with implant fixed complete dental prostheses in the edentulous mandible after at least 5 years: a systematic review, *Clin. Implant Dent. Relat. Res.* 16 (2014) 705–717, <https://doi.org/10.1111/cid.12036>.
- [2] C.J. Goodacre, G. Bernal, K. Rungcharassaeng, J.Y. Kan, Clinical complications with implants and implant prostheses, *J. Prosthet. Dent.* 90 (2003) 121–132, [https://doi.org/10.1016/s0022-3913\(03\)00212-9](https://doi.org/10.1016/s0022-3913(03)00212-9).
- [3] B.E. Pjetursson, D. Thoma, R. Jung, M. Zwahlen, A. Zembic, A systematic review of the survival and complication rates of implant-supported fixed dental prostheses (FDPs) after a mean observation period of at least 5 years, *Clin. Oral Implants Res.* 23 (6) (2012) 22–38, <https://doi.org/10.1111/j.1600-0501.2012.02546.x>, Suppl.
- [4] P. Papaspyridakos, C.J. Chen, G.O. Gallucci, A. Doukoudakis, H.P. Weber, V. Chronopoulos, Accuracy of implant impressions for partially and completely edentulous patients: a systematic review, *Int. J. Oral Maxillofac. Implants* 29 (2014) 836–845, <https://doi.org/10.11607/jomi.3625>.
- [5] P. Papaspyridakos, G.O. Gallucci, C.J. Chen, S. Hanssen, I. Naert, B. Vandenberghe, Digital versus conventional implant impressions for edentulous patients: accuracy outcomes, *Clin. Oral Implants Res.* 27 (2016) 465–472, <https://doi.org/10.1111/clr.12567>.
- [6] M. Perez-Davidi, M. Levit, O. Walter, Y. Eilat, P. Rosenfeld, Clinical accuracy outcomes of splinted and nonsplinted implant impression methods in dental residency settings, *Quintessence Int.* 47 (2016) 843–852, <https://doi.org/10.3290/j.qi.a36323>.
- [7] K. Miyoshi, S. Tanaka, S. Yokoyama, M. Sanda, K. Baba, Effects of different types of intraoral scanners and scanning ranges on the precision of digital implant impressions in edentulous maxilla: an *in vitro* study, *Clin. Oral Implants Res.* 31 (2020) 74–83, <https://doi.org/10.1111/clr.13548>.
- [8] K. Nagata, K. Fuchigami, Y. Okuhama, K. Wakamori, H. Tsuruoka, T. Nakashizu, N. Hoshi, M. Atsumi, K. Kimoto, H. Kawana, Comparison of digital and silicone impressions for single-tooth implants and two- and three-unit implants for a free-end edentulous saddle, *BMC Oral Health* 21 (2021) 464, <https://doi.org/10.1186/s12903-021-01836-1>.
- [9] G. Revell, B. Simon, A. Mennito, Z.P. Evans, W. Renne, M. Ludlow, J. Vag, Evaluation of complete-arch implant scanning with 5 different intraoral scanners in

- terms of trueness and operator experience, *J. Prosthet. Dent.* 128 (2022) 632–638, <https://doi.org/10.1016/j.prosdent.2021.01.013>.
- [10] M.Y. Tan, S.H.X. Yee, K.M. Wong, Y.H. Tan, K.B.C. Tan, Comparison of three-dimensional accuracy of digital and conventional implant impressions: effect of interimplant distance in an edentulous arch, *Int. J. Oral Maxillofac. Implants* 34 (2019) 366–380, <https://doi.org/10.11607/jomi.6855>.
- [11] M. Lyu, P. Di, Y. Lin, X. Jiang, Accuracy of impressions for multiple implants: a comparative study of digital and conventional techniques, *J. Prosthet. Dent.* 128 (2022) 1017–1023, <https://doi.org/10.1016/j.prosdent.2021.01.016>.
- [12] P. Thanasrisuebwong, T. Kulchotirat, C. Anunmana, Effects of inter-implant distance on the accuracy of intraoral scanner: an *in vitro* study, *J. Adv. Prosthodont.* 13 (2021) 107–116, <https://doi.org/10.4047/jap.2021.13.2.107>.
- [13] C.C.D. Resende, T.A.Q. Barbosa, G.F. Moura, L.D.N. Tavares, F.A.P. Rizzante, F. M. George, F.D.D. Neves, G. Mendonca, Influence of operator experience, scanner type, and scan size on 3D scans, *J. Prosthet. Dent.* 125 (2021) 294–299, <https://doi.org/10.1016/j.prosdent.2019.12.011>.
- [14] R. Huang, Y. Liu, B. Huang, C. Zhang, Z. Chen, Z. Li, Improved scanning accuracy with newly designed scan bodies: an *in vitro* study comparing digital versus conventional impression techniques for complete-arch implant rehabilitation, *Clin. Oral Implants Res.* 31 (2020) 625–633, <https://doi.org/10.1111/clr.13598>.
- [15] R. Huang, Y. Liu, B. Huang, F. Zhou, Z. Chen, Z. Li, Improved accuracy of digital implant impressions with newly designed scan bodies: an *in vivo* evaluation in beagle dogs, *BMC Oral Health* 21 (2021) 623, <https://doi.org/10.1186/s12903-021-01986-2>.
- [16] M. Iturrate, H. Eguiraun, E. Solaberrieta, Accuracy of digital impressions for implant-supported complete-arch prosthesis, using an auxiliary geometry part-an *in vitro* study, *Clin. Oral Implants Res.* 30 (2019) 1250–1258, <https://doi.org/10.1111/clr.13549>.
- [17] R.M. Mizumoto, B. Yilmaz, E.A. McGlumphy Jr., J. Seidt, W.M. Johnston, Accuracy of different digital scanning techniques and scan bodies for complete-arch implant-supported prostheses, *J. Prosthet. Dent.* 123 (2020) 96–104, <https://doi.org/10.1016/j.prosdent.2019.01.003>.
- [18] D. Borbola, G. Berkei, B. Simon, L. Romaszky, G. Sersli, M. DeFee, W. Renne, F. Mangano, J. Vag, *In vitro* comparison of five desktop scanners and an industrial scanner in the evaluation of an intraoral scanner accuracy, *J. Dent.* 129 (2023), 104391, <https://doi.org/10.1016/j.jdent.2022.104391>.
- [19] V. Rutkunas, A. Gedrimiene, M. Akulauskas, V. Fehmer, I. Sailer, D. Jelevecius, *In vitro* and *in vivo* accuracy of full-arch digital implant impressions, *Clin. Oral Implants Res.* 32 (2021) 1444–1454, <https://doi.org/10.1111/clr.13844>.
- [20] M. Iturrate, H. Eguiraun, O. Etxaniz, E. Solaberrieta, Accuracy analysis of complete-arch digital scans in edentulous arches when using an auxiliary geometric device, *J. Prosthet. Dent.* 121 (2019) 447–454, <https://doi.org/10.1016/j.prosdent.2018.09.017>.
- [21] T. Flugge, W.J. van der Meer, B.G. Gonzalez, K. Vach, D. Wismeijer, P. Wang, The accuracy of different dental impression techniques for implant-supported dental prostheses: a systematic review and meta-analysis, *Clin. Oral Implants Res.* 29 (16) (2018) 374–392, <https://doi.org/10.1111/clr.13273>. Suppl.
- [22] J.E. Kim, A. Amelya, Y. Shin, J.S. Shim, Accuracy of intraoral digital impressions using an artificial landmark, *J. Prosthet. Dent.* 117 (2017) 755–761, <https://doi.org/10.1016/j.prosdent.2016.09.016>.
- [23] R. Richert, A. Goujat, L. Venet, G. Viguie, S. Viennot, P. Robinson, J.C. Farges, M. Pages, M. Ducret, Intraoral scanner technologies: a review to make a successful impression, *J. Healthc. Eng.* 2017 (2017), 8427595, <https://doi.org/10.1155/2017/8427595>.
- [24] A.J. Ireland, C. McNamara, M.J. Clover, K. House, N. Wenger, M.E. Barbour, K. Alemzadeh, L. Zhang, J.R. Sandy, 3D surface imaging in dentistry - what we are looking at, *Br. Dent. J.* 205 (2008) 387–392, <https://doi.org/10.1038/sj.bdj.2008.845>.
- [25] P. Hong-Seok, S. Chintal, Development of high speed and high accuracy 3D dental intra oral scanner, *Procedia Eng.* 100 (2015) 1174–1181, <https://doi.org/10.1016/j.proeng.2015.01.481>.
- [26] O. Aubreton, A. Bajard, B. Verney, F. Truchetet, Infrared system for 3D scanning of metallic surfaces, *Mach. Vision. Appl.* 24 (2013) 1513–1524, <https://doi.org/10.1007/s00138-013-0487-z>.
- [27] J.J. Park, K. Kwon, N. Cho, Development of a coordinate measuring machine (CMM) touch probe using a multi-axis force sensor, *Meas. Sci. Technol.* 17 (2006) 2380–2386, <https://doi.org/10.1088/0957-0233/17/9/002>.
- [28] B. Alshawaf, H.P. Weber, M. Finkelman, K. El Rafie, Y. Kudara, P. Papispyridakos, Accuracy of printed casts generated from digital implant impressions versus stone casts from conventional implant impressions: a comparative *in vitro* study, *Clin. Oral Implants Res.* 29 (2018) 835–842, <https://doi.org/10.1111/clr.13297>.
- [29] F.S. Andriessen, D.R. Rijkens, W.J. van der Meer, D.W. Wismeijer, Applicability and accuracy of an intraoral scanner for scanning multiple implants in edentulous mandibles: a pilot study, *J. Prosthet. Dent.* 111 (2014) 186–194, <https://doi.org/10.1016/j.prosdent.2013.07.010>.
- [30] M. Sanda, K. Miyoshi, K. Baba, Trueness and precision of digital implant impressions by intraoral scanners: a literature review, *Int. J. Implant Dent.* 7 (2021) 97, <https://doi.org/10.1186/s40729-021-00352-9>.
- [31] J.F. Güth, D. Edelhoff, J. Schweiger, C. Keul, A new method for the evaluation of the accuracy of full-arch digital impressions *in vitro*, *Clin. Oral Investig.* 20 (2016) 1487–1494, <https://doi.org/10.1007/s00784-015-1626-x>.
- [32] B. Gimenez, M. Ozcan, F. Martinez-Rus, G. Pradies, Accuracy of a digital impression system based on parallel confocal laser technology for implants with consideration of operator experience and implant angulation and depth, *Int. J. Oral Maxillofac. Implants* 29 (2014) 853–862, <https://doi.org/10.11607/jomi.3343>.
- [33] A. Schmidt, C.R. Benedickt, M.A. Schlenz, P. Rehmann, B. Wöstmann, Torsion and linear accuracy in intraoral scans obtained with different scanning principles, *J. Prosthodont.* Res. 64 (2020) 167–174, <https://doi.org/10.1016/j.jpor.2019.06.006>.
- [34] P. Papispyridakos, Y.J. Kim, M. Finkelman, K. El-Rafie, H.P. Weber, Digital evaluation of three splinting materials used to fabricate verification jigs for full-arch implant prostheses: a comparative study, *J. Esthet. Restor. Dent.* 29 (2017) 102–109, <https://doi.org/10.1111/jerd.12274>.
- [35] E.D. de Avila, F. de Matos Moraes, S.M. Castanharo, M.A. Del'Acqua, F. de Assis Mollo Jr., Effect of splinting in accuracy of two implant impression techniques, *J. Oral Implantol.* 40 (2014) 633–639, <https://doi.org/10.1563/AAID-JOI-D-12-00198>.
- [36] V. Rutkunas, V. Bilius, T. Simonaitis, L. Auskalnis, J. Jurgilevicius, M. Akulauskas, The effect of different implant impression splinting techniques and time on the dimensional accuracy: an *in vitro* study, *J. Dent.* 126 (2022), 104267, <https://doi.org/10.1016/j.jdent.2022.104267>.
- [37] P. Marx, A. Romano, I. Roppolo, A. Chemelli, I. Mühlbacher, W. Kern, S. Chaudhary, T. Andritsch, M. Sangermano, F. Wiesbrock, 3D-printing of high-κ thiol-ene resins with spiro-orthoesters as anti-shrinkage additive, *Macromol. Mater. Eng.* 304 (2019), <https://doi.org/10.1002/mame.201900515>.